Cosmic ray electron anisotropies as a tool to discriminate between exotic and astrophysical sources

Ignacio Cernuda

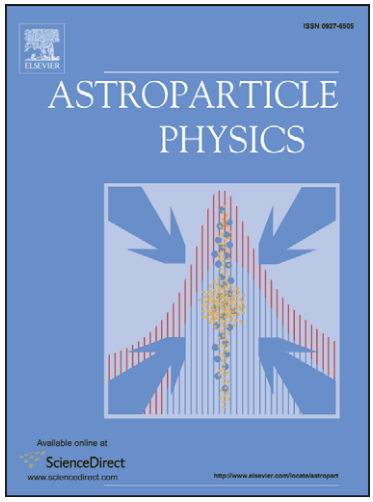

Cosmic ray electron anisotropies as a tool to discriminate between exotic and astrophysical sources

Ignacio Cernuda

PII: S0927-6505(10)00099-X
DOI: 10.1016/j.astropartphys.2010.05.003
Reference: ASTPHY 1494

To appear in: *Astroparticle Physics*

Received Date: 8 May 2009
Revised Date: 26 April 2010
Accepted Date: 18 May 2010

Please cite this article as: I. Cernuda, Cosmic ray electron anisotropies as a tool to discriminate between exotic and astrophysical sources, *Astroparticle Physics* (2010), doi: 10.1016/j.astropartphys.2010.05.003

Cosmic ray electron anisotropies as a tool to discriminate between exotic and astrophysical sources.

Ignacio Cernuda

Basic Research Division, Centro de Investigaciones Energéticas, Medioambientales y Tecnológicas (CIEMAT***) Avda. Complutense, 22 - 28040 Madrid,Spain***

Abstract

Recent results from the PAMELA [1], ATIC [2], PPB BETS [3] and Fermi [4] collaborations extend the energy range in the e^+, e^- measurement up to unexplored energies in the hundreds of GeV range confirming the bump starting at about 10 GeV already suggested by HEAT [5] and AMS01 data [6]. This bump can be explained by the annihilation of dark matter (DM) in the context of exotic physics, or by nearby astrophysical sources such as pulsars. In order to discriminate between the competing models for primary positron production, the study of anisotropies, in addition to the spectrum determination, shows up as new tool for investigating the origin of the lepton excess. In this letter we calculate the contribution to the electron flux due to both the collection of all known Gamma-Ray pulsars (as listed in the ATNF catalogue) and by the annihilation of dark matter. In the latter case we consider that the excess can be attributed to a clumpy halo or a nearby sizeable dark matter clump. We address the problem of the electron anisotropy in both scenarios and estimate the prospect that a small dipole anisotropy might be found by the Fermi observatory.

Keywords:
Dark Matter, Anisotropy, Pulsar, PAMELA, ATIC, Fermi/LAT

Email address: ignacio.cernuda@ciemat.es (**Ignacio Cernuda**)

1. Introduction

The recent claim from the PAMELA collaboration of an excess in the ratio of positrons to electrons plus positrons (positron fraction) seems to support what HEAT and AMS01 data suggested regarding the existence of a possible primary cosmic ray electrons source. However some uncertainties remain, e.g. the possible enhancement of the positron flux due to the relative poor knowledge of the propagation parameters set [7].

A large number of candidates have been suggested that might be able to reproduce the observed positron fraction. Among the exotic ones, the annihilation of dark matter may be the most widely studied. Dark matter is assumed to annihilate in the galactic halo and its annihilation products should be measurable from Earth. As it has been pointed out in previous works [8], PAMELA data seems to accommodate preferably leptonic channels rather than dark matter annihilating to quark pairs, but typically large boost factors are required to adjust the shape to the data. These boost factors are related to an increase of the annihilation rate which can be explained for instance by the recently invoked Sommerfeld effect, annihilation of a non thermal WIMP, or the usual inhomogeneities of the dark matter halo (clumps, dark matter mini spikes etc). Moreover, to accommodate theory to the existing data, different normalizations are required for the different experiments.

More conventional scenarios such as pair production in nearby astrophysical objects can also reproduce the spectral shape. Specifically in this work, we analyze the possible contribution of pulsars and leptophilic dark matter. The Fermi data can be easily reproduced by pulsars with standard parameterizations owing to its flat spectrum. On the contrary, the ATIC data presents a spiky shape that can be explained in the case of multiple sources. Namely, the presence of peaks in the spectrum can be reproduced given a convenient selection of pulsars, or for a distribution of DM clumps contributing to the total flux with the required luminosity. However, in order to do so it is necessary to fine tune the pulsar parameters to fit the peaks present in the ATIC spectrum.

In this paper we calculate the predicted dipole anisotropy produced in both scenarios, i.e., dark matter annihilation and nearby pulsars, and assess the Fermi detection capability of such signature at least at the 2 sigma confidence level.

2. Propagation

Cosmic ray propagation is a diffusive process due to the random galactic magnetic fields. If we denote the number of particles of type i per unit volume found at time t at $\vec{x}$ with energy E by $n_i(E,\vec{x},t)$ $[GeV^{-1}cm^{-3}]$, the evolution equation as initially written by *Ginzburg* and *Syrotvatskii* [9] can be expressed as:

$$\begin{aligned}\frac{\partial n_i}{\partial t} &= \nabla(\mathbf{D}\nabla n_i) - \nabla(\vec{v}n_i) - \frac{\partial}{\partial E}(bn_i) \\ &+ \beta cN\sum_{s<i} n_s\sigma_{i,s} - \beta cN\sigma_i n_i - \frac{n_i}{\Gamma\tau_i} + Q_i \end{aligned} \quad (1)$$

where $\nabla(\mathbf{D}\nabla n_i)$ is the diffusion term and $\mathbf{D}(E,\vec{x},t)$ [cm^2/s] is the diffusion tensor; $\nabla(\vec{v}n_i)$ is the convection term and $\vec{v}=\vec{v}(\vec{x})$ [cm/s] is the velocity of the galactic wind; $\frac{\partial}{\partial E}(bn_i)$ represents the energy loss with $b(E,\vec{x},t)$ [GeV/s] being the rate of energy change; $\frac{n_i}{\Gamma\tau_i}$ is the fraction of particles lost by radioactive decay with a characteristic life-time τ_i [s] and $\beta cN\sum_{s<i} n_s\sigma_{i,s} - \beta cN\sigma_i n_i$ is the number density of particles created or destroyed by spallation processes in the propagation due to interactions with the interstellar medium of density N, with a cross section $\sigma_{i,s}$ [cm^2]. Finally, we have the source term $Q_i(E,\vec{x},t)$ [GeV^{-1}cm^{-3}s^{-1}] that describes the injection of particles of type i into the Galaxy.

For electron and positron propagation, the relevant processes are diffusion, convection, energy losses and the source term. Propagation can be approached in two complementary ways. The first one is to solve the transport equation using numerical methods in the same way the package *GALPROP* [10] does. The second one is to analytically solve the transport equation with a set of realistic simplifying assumptions. In this work we use the standard *GALPROP* code to get the positron and electron backgrounds and an analytical solution of the propagation equation for the primary positron flux. For primary positron sources, we have used the Green functions formalism as described in [11] where the two main processes, diffusion and energy losses, are considered. The resulting diffusion-loss equation for this process is given by:

$$\begin{aligned}\frac{\partial}{\partial t}n(E,\vec{x},t) &= D(E)\cdot\nabla^2 n(E,\vec{x},t) \\ &- \frac{\partial}{\partial E}(b(E)n(E,\vec{x},t)) + Q(E,\vec{x},t)\end{aligned} \quad (2)$$

Where $b(E) = -\frac{dE}{dt} = aE^2 + bE + c \approx aE^2$ codifies the energy losses due to (a) inverse Compton scattering (IC) and synchrotron radiation, (b) bremsstrahlung and (c) ionization. At the energies we are interested in, E > 10 GeV, the energy loss is very well approximated by the synchrotron losses in the interstellar (ISM) magnetic fields and inverse Compton scattering off the background radiation (Cosmic Microwave Background radiation (CMB) and starlight at optical and IR frequencies). The energy loss due to these processes is calculated as [9]:

$$\begin{aligned} -\frac{dE}{dt} &= \frac{32\pi}{9} c \left(\frac{e^2}{mc}\right)^2 \left(w_0 + \frac{B^2}{8\pi}\right) \left(\frac{E}{mc^2}\right)^2 \\ &= 8\text{x}10^{-17} \left(\text{w}_0 + 6\text{x}10^{11} \frac{(\text{B}/1\text{G})^2}{8\pi}\right) \text{E}^2 \approx 10^{-16} \text{E}^2 [\text{GeVs}^{-1}] \end{aligned} \quad (3)$$

where the energy density $w_0 = w_{CMB} + w_{opt-IR}$ is the energy density of the photon background $[eV/cm^3]$ with $w_{CMB} = 0.25$ eV/cm^3 and $\text{w}_{\text{opt}-\text{IR}} = 0.5$ eV/cm^3. w_B stands for the ISM magnetic field energy density $w_B = \frac{B^2}{8\pi} = 0.6$ eV/cm^3 for B=5μG.
For the diffusion coefficient $D(E) = D_0 E^\gamma$, three setups MAX,MED and MIN, which are consistent with measurements of the boron to carbon ratio B/C can be considered [7].

Table 1: Diffusion Setups

	D_0 $[cm^2/s]$	γ
MAX	1.8×10^{27}	0.55
MED	3.4×10^{27}	0.70
MIN	2.3×10^{28}	0.46

We solve the equation for a steady state source (DM positron injection) and for a non-stationary source (SNRs and pulsars) assuming free boundary conditions.

3. Astrophysical sources of high energy positrons

Among the astrophysical objects that populate our Galaxy, many can contribute to the positron abundance in cosmic rays, but the required energy excludes a large part of them. Following a Hillas-like argument, the

astrophysical sources able to inject the required order of energy can be found in e.g: SNRs and pulsars.

Gamma-Ray pulsars are expected to produce pairs of electrons and positrons as a result of electromagnetic cascades induced by the acceleration of electrons in the magnetosphere. There are two main mechanisms of pulsar particle acceleration with the subsequent radiation emission and pair production processes, namely the polar cap and the outer gap models. We will not detail these mechanisms in this work. In short, in both models the electrons can be accelerated to ultrarelativistic energies by electric fields in the magnetosphere of the pulsar. These electrons emit synchrotron and/or curvature radiation with energies large enough to produce electron-positron pairs in the strong magnetic field of the pulsar magnetosphere by magnetic conversion, and/or through photon-photon pair production with photons from the local radiation fields such as thermal X-rays from the neutron star surface. It is then reasonable to think that the physical process that produces e^+e^- in the pulsar magnetosphere is presumably the same that produces the Gamma-Ray emission [12], although additional processes such as reacceleration in the pulsar wind nebula should be taken into account. We assume that the positron injection spectrum can be expressed as a power-law with an exponential cutoff at E_c, $\frac{dN_e}{dE} = E^{-\alpha}e^{-E/Ec}$.

Previous works (e.g. [12], [13], [14], [15], [16],[17], [18], [19]) have shown the plausibility of the pulsar scenario as sources of primary cosmic ray electrons. In our analysis, we will assume a benchmark model as considered in [18], namely, the "standard model" (ST). Although more refined models for electron production in pulsars can be considered, some of them produce an $e^{\pm}$ output well below the observations (e.g. Harding-Ramaty model [12] or the one devised by Zhang and Cheng [20]) or a comparable one (e.g. Chi et al. [16]). In the latter case, the most outstanding pulsars produce similar patterns to those considered in the ST model, so we will assume the most simple scenario for positron production in pulsars as a benchmark model for the study.

The ST model assumes that all the rotational energy of the pulsar is lost through magnetic dipole radiation. Since the rotational energy is given by $E = I\Omega^2/2$ (where I$\approx 10^{45} gcm^2$ is the moment of inertia and Ω the spin frequency), the spin-down power will be $\dot{E} = I\Omega\dot{\Omega}$. For such a magnetic dipole radiator, the energy loss rate can be written as a function of the neutron star's radius R, and α the angle between the dipole and rotation axes $\dot{E} = -\frac{B^2R^6\Omega^4\sin^2\alpha}{6c^3}$, i.e. $\dot{\Omega} \propto -\Omega^3$. Integrating this expression leads to the

solution of the time evolution of the rotational velocity of a pulsar for which the magnetic dipole radiation braking dominates:

$$\Omega(t) = \frac{\Omega_0}{(1 + t/\tau_0)^{1/2}} \tag{4}$$

where Ω_0 is the initial spin frequency and $\tau_0 = \frac{3c^3 I}{B^2 R^6 \Omega_0^2}$ is a characteristic time taken to be around 10^4 years for nominal pulsar parameters. Using Eq. 4, we obtain the spin-down power $\dot{E}$ of the pulsar.

$$\dot{E} = I\Omega\dot{\Omega} = \frac{1}{2} I\Omega_0^2 \frac{1}{\tau_0} \frac{1}{(1 + t/\tau_0)^2} \tag{5}$$

If we assume that a fraction $f_{e^\pm}$ of the spin-down power $\dot{E}$ is translated into pair production, then, we can describe the power injected into $e^\pm$ by a luminosity function $\mathcal{L}_{e^\pm}$ as:

$$\mathcal{L}_{e^\pm}(t) = f_{e^\pm} \dot{E} = \frac{\mathcal{L}_0}{(1 + t/\tau_0)^2} \tag{6}$$

where $\mathcal{L}_0 = f_{e^\pm} \frac{1}{2\tau_0} I\Omega_0^2$.
Integrating Eq. 5 over the pulsar age T, the total energy output can be approximated by $E_{out} = I \int dt \Omega\dot{\Omega} \approx I\Omega_0/2$. If $t/\tau_0 >> 1$ then $\Omega_0^2 \simeq \Omega^2 \frac{t}{\tau_0}$ leads to an energy output into electrons of:

$$E_{out}[ST] = f_{e^\pm} \dot{E} \frac{T^2}{\tau_0} \tag{7}$$

where the energy budget is determined by the present spin-down power $\dot{\mathrm{E}}$, the age of the source T and the conversion efficiency into pairs $f_{e^\pm}$ that is assumed to be of a few percent. Thus, the $e^\pm$ source for a single pulsar located at a distance r, injecting positrons at time t and energy E can be expressed as:

$$Q(E, r, t) = Q_0 \cdot \mathcal{L}_{e^\pm}(t) E^{-\alpha} \exp\left(-E/E_c\right) \delta(r) \tag{8}$$

where Q_0 is the normalization factor taken to satisfy the total energy release constraint $E_{tot} = \int^T d\tau \int_{1GeV}^{E_{max}} EQ(E, \tau) dE$ and $\mathcal{L}_{e^\pm}$ is the luminosity of the source. We have introduced a spectral cutoff at E_c=1TeV motivated by the ATIC and Hess data. This cutoff will only be relevant for young pulsars, as old pulsars have a maximal $e^\pm$ energy below the cutoff due to

energy losses. In this work we have assumed typical pulsar injection for magnetic dipole radiation braking (Eq. 5), nonetheless a similar analysis can be conducted for other choices e.g. exponential decay luminosity as it is expected from microquasars or $e^{\pm}$ release from the nebula surrounding pulsars.

Once we have described the source of electrons from a single pulsar, we proceed to estimate the contribution to the local e^+e^- flux from a realistic collection of Gamma-Ray pulsars. For this purpose we will consider all the Gamma-Ray pulsars listed in the Australian Telescope National Facility (ATNF) [21] pulsar catalogue [1]. Young pulsars with typical ages lower than $10^4 - 10^5$ years are considered to be surrounded by a pulsar wind nebula (PWN) or a SNR shell that confines the injected electrons before releasing them to the ISM. This has to be taken into account when we consider the age of the pulsars that can contribute to the electron abundance. In this respect we will consider two collections. In the first one we will take a lower bound of 10^4 years constraining our pulsar collection to ages between 10^4 and 10^7 years (Table 3). This constraint allows us to accept pulsars like Vela which is still surrounded by a PWN. In this scenario, we assume a low conversion efficiency for the young pulsars ($\mathcal{O}(1\%)$) to take into account the possible confinement of leptons. In the second one, we will consider that pulsars with ages lower than 5x10^4 years cannot contribute to the bulk of electrons, i.e. we constrain our collection to mature pulsars. This introduces an injection delay Δt between the pulsar's birth and the injection of electrons into the ISM due to their confinement in the PWN. This delay may be relevant for young pulsars for which $T \simeq \Delta t$ but for sufficiently old pulsars we can safely dismiss the delay issue and set the injection time at the pulsar age.
The condition for Gamma-Ray emission as described in [22] is that the fraction size of the outer gap be less than one, $g = 5.5 P^{26/21} B_{12}^{-4/7} < 1$ in terms of the pulsar period P and the pulsar surface magnetic field B_{12} (in $10^{12} G$ units) resulting in a collection of more than two hundred pulsars, from which three lie at a distance closer than 1kpc. Regarding the determination of the injection spectral index α, we have to take into account the constraints that come from observations of synchrotron radiation from SNRs. We can consider, as in the Harding-Ramaty model [18], that the $e^{\pm}$ have the same spectral index as Gamma-Rays emitted by pulsars (which has been measured

[1] http://www.atnf.csiro.au/research/pulsar/psrcat

by EGRET to be around 1.4-2.2 for energies $0.1 < E < 10$ GeV [23]). This is a fairly large range, so for the sake of simplicity we will assume that our collection of pulsars have all the same spectral index $\alpha = 1.7$ provided that with this configuration we get reasonable fits to the data (e.g. [19]). As an additional simplifying assumption we will take a universal set of parameters for the whole collection. This way, neither the PAMELA nor ATIC data can be reproduced properly, but with a little fine tuning, their spectral features can be obtained. For instance, as recently pointed out by [24], the width of the peak produced by continuous injection depends on the characteristic time of the luminosity of the pulsar by $\frac{\Delta\epsilon_{peak}}{\epsilon_{peak}} \simeq \frac{\tau_0}{T}$. Proceeding like this, selecting a number of well known pulsars and adjusting their luminosity parameters, the spiky spectral shape of ATIC can be achieved without violating the PAMELA constraints. Additionally, the energy losses determine the age of the source that produces the peak around 600 GeV reported by ATIC, provided that it is far ($\sim 1Kpc$) and bright enough (~ 1 order of magnitude in the conversion efficiency). As already noted by [18], PSR B0355+54 fulfills the requirements. For this pulsar, a very large conversion efficiency into pairs is required to account for the ATIC peak ($\mathcal{O}(40\%)$). On the other hand, the much more statistically significant Fermi/LAT data shows a considerably flatter spectrum. Just taking standard pulsar parameters is enough to fit the data without having to resort to very large conversion efficiencies so this is the approach we will follow, although it should be noted that due to the poor Fermi energy resolution at these energies, actually existing peaks could be smoothed down to the observed spectrum, proving the issue of normalization of every pulsar to be a subtle one.

Once we have the positron source we proceed to calculate the number density of positrons by solving the diffusion-loss equation (Eq.2) for a non stationary source. The solution of the equation has been previously derived for a burstlike power-law injection source with a cutoff E_c ([25], [19]).

$$\phi(E,r,t) = \frac{\beta c}{4\pi}\frac{Q_0}{\pi^{3/2}r^3}\left(\frac{r}{D_{diff}}\right)^3 (1-atE)^{\alpha-2}E^{-\alpha}e^{-\frac{E}{(1-atE)E_c}}e^{-\left(\frac{r}{D_{diff}}\right)^2} \quad (9)$$

where the distance scale is approximately,

$$D_{diff}(E,t) \simeq 2\sqrt{D(E)t\frac{1-(1-E/E_{max})^{1-\gamma}}{(1-\gamma)E/E_{max}}} \tag{10}$$

as a function of the index of the power-law dependence of the diffusion term on energy, γ, and the maximum energy given by the energy losses: $E_{max} \simeq 1/(at)$ with $a \simeq 10^{-16}$ GeV^{-1}s^{-1}.

Given that the source emits with luminosity $\mathcal{L}_{e^\pm}(t)$, the flux will be given by $\phi(E,r,t) = \int_T^t \mathcal{L}_{e^\pm}(t')\phi(E,r,t')dt'$. We have calculated the pulsar contribution to the local electron flux in the case of burstlike injection and continuous injection for our collection of young and mature pulsars. Even in the continuous case, the injection is well approximated by a burstlike event as a result of the steepness of the slope of the luminosity function for a braking index due to magnetic dipole radiation. In this case, a broader peak in the spectrum is produced because a significant fraction of the electrons are released recently, thus having a shorter cooling time and reaching Earth with a higher energy [24]. In order to reproduce the spectral features of the Fermi data, we assume a MED diffusion scenario with an overall conversion efficiency of 3%. Due to the relative variability of the collection of pulsars in the age/distance parameter space, we adjust the conversion efficiency for a few number of objects that show prominent features in the spectrum at the considered energies, namely Geminga, Monogem and J2043+2740 (Fig. 1).

We can consider two sets of pulsars (BM1,BM2) to address the lepton confinement in the PWN. Our first set will be made up of mature pulsars with ages T> 5x10^4 years, thus introducing a delay between the pulsar birth and the electron release to the interstellar medium of $\Delta t \simeq$ 5x10^4 years. In our second set, we also consider younger pulsars, including Vela, with ages T> 10^4 years and a delay of $\Delta t \simeq 10^4$ years. In this scenario, as young pulsars are still surrounded by the nebula that confines the electrons, a smaller efficiency must be called for. The efficiency we will assume for these pulsars, including Vela, is $\mathcal{O}(1\%)$, and is taken to satisfy the bounds imposed by the Hess data. A larger efficiency would imply a non negligible contribution above the background of secondary electrons around 2 TeV due to the contribution of Vela, which has not been not observed.

The resulting fluxes are shown (Figs. 2 and 3) for the considered scenarios. In order to account for the experimental data in the hundreds of GeV, the

conversion efficiency into pairs of Monogem and Geminga must be above the nominal value of 3% but inside the standard range (1-30%) considered in [26]. This values may change depending on the diffusion setup considered, the PWN $e^{\pm}$ release delay, pulsar cutoff, etc so it should be considered as a single realization of the multiple possibilities that can reproduce the data [19].

4. Dark Matter source of high energy positrons

According to the standard ΛCDM cosmological model, approximately a 22% of the energy content of the universe is in the form of cold dark matter (CDM). Probably the leading candidates to account for it are weakly interacting particles (WIMPS), with the neutralino and the Kaluza-Klein boson B^1 the most extensively studied ones. The relic density of these particles is determined by their annihilation cross section. Observations of the

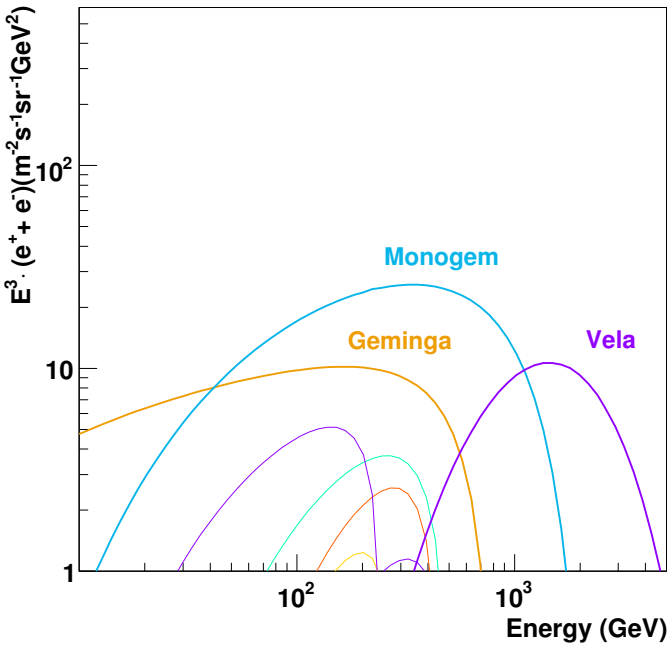

Figure 1: Contribution to the electron flux by the collection of pulsars considered in the BM2 setup , Table 3.

Table 2: Pulsar Parameters

Pulsar	d[Kpc]	T [10^5 years]	E_{out} BM1/BM2 [10^{47}erg]	$f_{e^\pm}$ BM1/BM2 [%]
Geminga	0.16	3.42	11.9/7.0	10.0/6.0
Monogem	0.29	1.11	2.7/4.5	18.0/30.0
J2043+2740	1.13	12.0	2.6/2.6	0.1/0.1
Vela	0.29	0.11	0.0/0.3	0.0/1.0

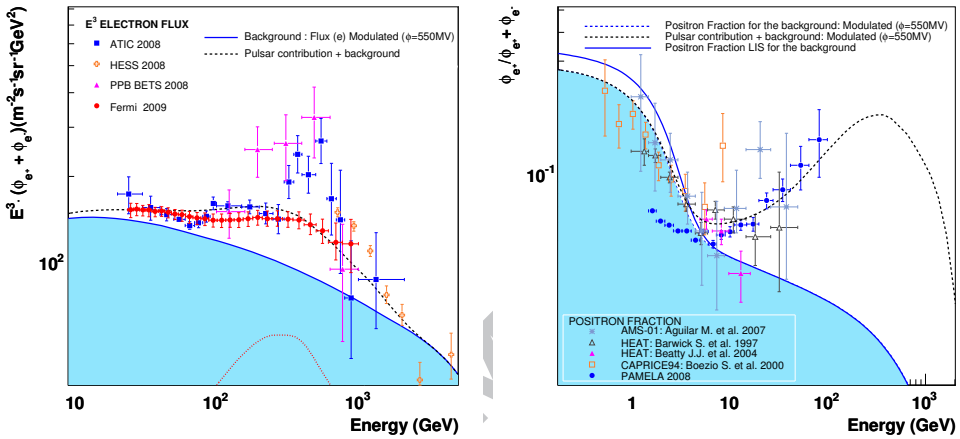

(a) (b)

Figure 2: Mature pulsar contribution to the electron flux (pulsar contribution to the total flux in red dashed line, background in blue solid line and pulsar contribution + background in black dashed line. The blue dashed line that bounds the blue flooded area denotes a modulated positron fraction for the background.) for a MED diffusion setup and overall efficiency $f_{e^\pm} = 3\%$. We assume an injection index of $\alpha = 1.7$ and a cutoff $E_c = 1$ TeV. We consider burstlike injection and the efficiencies have been adjusted to $f_{\pm e}^{Monogem} = 18\%$, $f_{\pm e}^{Geminga} = 10\%$, $f_{\pm e}^{J2043+2740} = 0.1\%$ to reproduce the Fermi and PAMELA data. (a): $E^3 \cdot (e^+ + e^-)$ (b): Positron Fraction

CMB and large scale structure surveys provide estimates of the relic density constraining the annihilation cross section up to a canonical value of $\langle \sigma v \rangle \approx 3 \times 10^{-26}$ cm^{3}s^{-1}. This value sets the production rate of standard model particles, e.g. leptons, that can be measured as tracers of dark matter annihilation.

The signal that results from DM annihilation, depends on the squared DM density from the astrophysical side, and on the DM particle mass and cross section from the particle physics side. Since the annihilation rate depends

on the squared density, the presence of clumpiness or substructure implies an enhancement of the signal compared to a smooth density distribution. The present dark matter structure is considered to have its roots in small amplitude quantum fluctuations during inflation. In the accepted "bottom-up" hierarchical structure formation, smaller clumps gather together to form larger systems, completely determined by the initial power spectrum of the primordial fluctuations. Galaxies are thus embedded in large dark matter halos that in turn are made up of self-bound substructure or subhalos. The mass distribution, abundance and internal structure of clumps is determined by means of high-resolution numerical simulations as the one conducted by Diemand et al.[27]. In this work we make use of the mass distribution of clumps that results from Diemand et al.'s simulation as in Cumberbatch et al. [28] expressed as:

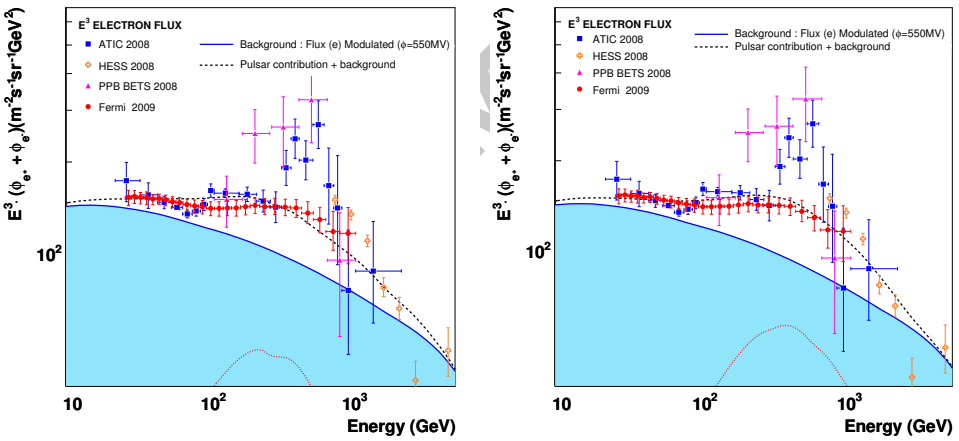

(a) (b)

Figure 3: Pulsar contribution to the total flux in red dashed line, background in blue solid line and pulsar contribution + background in black dashed line. (a):Mature + young pulsar contribution to the $e^+ + e^-$ flux for a MED diffusion setup, burstlike injection and $f_{e^\pm} = 3\%$. We have considered an injection index of $\alpha = 1.7$ and a cutoff $E_c = 1$ TeV.The efficiencies have been adjusted to $f^{\pm e}_{Monogem} = 30\%$, $f^{\pm e}_{Geminga} = 6\%$, $f^{\pm e}_{J2043+2740} = 0.1\%$, $f^{\pm e}_{Vela} = 1\%$ to reproduce the Fermi data. (b): Mature pulsar contribution to the $e^+ + e^-$ flux for a MED diffusion setup, continuous injection and overall efficiency $f_{e^\pm} = 3\%$. We assume an injection index of $\alpha = 1.7$ and a cutoff $E_c = 1TeV$. The efficiencies have been adjusted to $f^{\pm e}_{Monogem} = 15\%$, $f^{\pm e}_{Geminga} = 6\%$, $f^{\pm e}_{J2043+2740} = 0.1\%$ to reproduce the Fermi data.

$$\frac{dn_D}{d\log(M/M_\odot)} \;\alpha\; (M/M_\odot)^{-1}\exp[-(M/M_{cutoff})^{-2/3}] \tag{11}$$

where the lower mass cutoff is $M_{cutoff} \simeq 8.03\text{x}10^{-6}\text{M}_\odot$ and, inspired by Diemand et al.'s simulation, we take an upper mass cutoff at $10^{10}M_\odot$. We normalize the distribution such that we have a local clump density (r=$r_\odot = 8.5Kpc$) of $500\,pc^{-3}$ between $10^{-6}M_\odot$ and $10^{-5}M_\odot$. For the spatially dependent number density we assume a spherically symmetrical Navarro, Frenk and White (NFW) profile so the density of clumps is given by

$$\frac{dn(r,M)}{d\log(M/M_\odot)} = \frac{\rho_0}{(r/R)[1+(r/R)]^2}\frac{dn_D}{d\log(M/M_\odot)} \tag{12}$$

where $R = 20$ Kpc and $\rho_0 = 0.86$ for a correct normalization.

For the internal structure within a clump, we adopt a NFW density profile that gives a reasonable fit to the lightest clumps in Diemand et al.'s simulation and reproduces well the outer parts of the large scale subhalos.

$$\rho(r) = \frac{\rho_0}{c(r/r_{200})[1+c(r/r_{200})]^2} \tag{13}$$

where the maximum radius of the clump is defined as the radius r_{200} where the density equals 200 times the critical density. We assume a universal concentration parameter c for all the clumps, found to lie in Diemand et al.'s simulation within the $1.6 \leq c \leq 3.0$ range, and a constant density core below 10^{-9} Kpc.

With all these considerations, the source term can be expressed as:

$$Q(E,r) = \frac{\langle\sigma v\rangle}{m_{DM}^2} \qquad f(E)\int_{M_{min}}^{M_{max}} f_{NFW}^2(c,M) \frac{dn(r,M)}{d\log(M/M_\odot)} d\log(M/M_\odot) \tag{14}$$

where f(E) denotes the number of positrons generated per annihilation and energy interval (for each branching channel) and $f_{NFW}^2(c,M)$ is the integrated squared density for each DM clump

$$f_{NFW}^2(c,M) = \int_0^{r_{200}(M)} 4\pi r'^2\rho^2(r')dr' \tag{15}$$

Once we have the source term we proceed to calculate the flux at the Earth by solving the steady state ($\frac{\partial}{\partial t} n(E, \vec{x}) = 0$) of Eq.2. As already done e.g in [29], the equation can be solved turning the energy evolution into an evolution over a pseudo-time $\tilde{t}$.

$$\tilde{t} = \tau_E \left\{ \frac{E^{\gamma-1}}{1-\gamma} \right\} \tag{16}$$

where $\tau_E \equiv 1/a = 10^{16} GeV s$ and γ is the exponent of the energy dependence of the diffusion index.

The equation then reads:

$$\frac{\partial \psi}{\partial \tilde{t}} - D_0 \Delta \psi = \tilde{Q}(\vec{x}, \tilde{t}) \tag{17}$$

where $\psi = E^2 n$ and $\tilde{Q} = E^{2-\gamma} Q$. This equation is analogous to the heat equation with positrons evolving with the pseudo-time $\tilde{t}$. The solution of this equation can be obtained in the Green function formalism, where the probability for a positron with monochromatic injection energy E_s initially located at $\vec{x}_s$ to reach the observer position $\vec{x}$ with energy $E \leq E_s$, is described by the Green function $G(\vec{x}, E \leftarrow \vec{x}_s, E_s)$. The solution is then given by the convolution of the Green function over the sources $Q(\vec{x}_s, E_s)$.

$$n(\vec{x}, E) = \int_E^\infty dE_s \int_{Halo} d^3\vec{x}_s G(\vec{x}, E \leftarrow \vec{x}_s, E_s) Q(\vec{x}_s, E_s) \tag{18}$$

We can relate the positron propagator $G(\vec{x}, E \leftarrow \vec{x}_s, E_s)$ with the propagator of the heat equation $\tilde{G}(\vec{x}, \tilde{t} \leftarrow \vec{x}_s, \tilde{t}_s)$

$$G(\vec{x}, E \leftarrow \vec{x}_s, E_s) = \frac{\tau_E}{E^2} \tilde{G}(\vec{x}, \tilde{t} \leftarrow \vec{x}_s, \tilde{t}_s) \tag{19}$$

where the propagator of the 3D heat equation is just

$$\tilde{G}(\vec{x},\tilde{t}\leftarrow\vec{x}_s,\tilde{t}_s)=\left\{\frac{1}{4\pi D_0(\tilde{t}-\tilde{t}_s)}\right\}^{3/2}\exp\left\{-\frac{(\vec{x}-\vec{x}_s)^2}{4D_0(\tilde{t}-\tilde{t}_s)}\right\} \quad (20)$$

with a typical diffusion length $D_{diff}=\sqrt{4D_0(\tilde{t}-\tilde{t}_s)}$
The positron flux at the Earth is then $\phi_\odot(E)=\frac{\beta c}{4\pi}n(\vec{x}_\odot,E)$

$$\phi_\odot(E)=\frac{\beta c}{4\pi}\frac{\tau_E}{E^2}\int_E^\infty dE_s\int d^3\vec{x}_s\left\{\frac{1}{\frac{4\pi D_0\tau_E}{1-\gamma}(E^{\gamma-1}-E_s^{\gamma-1})}\right\}^{3/2}\exp\left\{-\frac{(\vec{x}_\odot-\vec{x}_s)^2}{\frac{4D_0\tau_E}{1-\gamma}(E^{\gamma-1}-E_s^{\gamma-1})}\right\}Q(\vec{x}_s,E_s) \quad (21)$$

As previously stated, PAMELA data favours leptophilic DM, i.e., candidates whose annihilation products are predominantly leptons. The case of direct annihilation into electron and positron pairs can provide good fits to the ATIC data but it must be excluded if we take into account the Fermi results due to a sharp drop at the end-point (see e.g. [30]). Therefore we are left with annihilations into $\mu^\pm$ and $\tau^\pm$ which provide a much softer injection spectrum and can accommodate both PAMELA and Fermi. For such injection spectra, large annihilation rates are required. The astrophysical boost factor, i.e, boost based on the presence of clumpiness, has been proved to be insufficient to account for the required normalization to adjust the data. In this respect, proposals of particle physics boost factors as velocity dependent cross sections, have been recently considered.
In this work our purpose is to evaluate the expected anisotropy resulting from sources that reproduces the observed abundances, so we will assume the required normalization to fit the data as a result of any of the considered mechanisms that can boost the annihilation rate. Here, we consider a DM candidate that annihilates into $\tau^\pm$ with a mass of 3.6 TeV (Fig. 4).

We also address the possibility of a nearby DM clump being the responsible of the bulk of positrons found in the Fermi, ATIC and PAMELA data. For this purpose, we treat here the clump as a point-like object at a given distance d contributing to the source term with luminosity L in the same fashion as already done in [31]. This possibility has been found to be very unlikely unless the Sommerfeld effect is at play, but such a source would

imprint a signature in the electron arrival direction that could constitute a signal of dark matter annihilation in case of the absence of pulsars in the neighbourhood. In this sense, the evaluation of such a signal makes the study meaningful. The expected flux for a clump of DM annihilating into $\tau^{\pm}$ or $\mu^{\pm}$ with masses around 3 TeV and 2 TeV respectively can reproduce the Fermi data with the drop observed by Hess, and with slightly different normalizations the PAMELA data. As a possibility, we show the flux produced by the annihilation in the $\tau^{\pm}$ channel of a DM clump located at 0.9 Kpc with a DM mass of 3.6 TeV. In this case, as in a pulsar scenario, a MED diffusion setup is appropriate, as the MIN and MAX cases show prominent bumps in the spectrum at high and low energies respectively, that are not observed in the Fermi data.

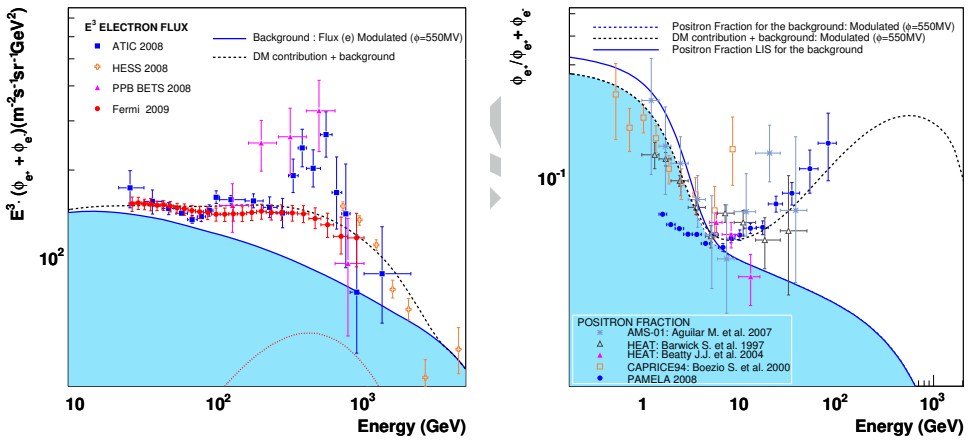

(a) (b)

Figure 4: DM clumpy halo contribution to the electron spectrum as described in the text. In each figure the blue solid line stands for the background whereas the black dashed line accounts for the DM contribution over the background to the total flux. The red dashed line denotes the DM contribution to the total flux. The blue dashed line that bounds the blue flooded area denotes a modulated positron fraction for the background. Annihilation into $\tau^+\tau^-$ with a cross section $\langle\sigma v\rangle = 4.65\text{x}10^{-24}\text{cm}^3/\text{s}$. The considered DM mass $M_{DM} = 3.6$ TeV and concentration parameter c=1.6. MED diffusion setup. (a): $E^3 \cdot (e^+ + e^-)$ (b): Positron Fraction

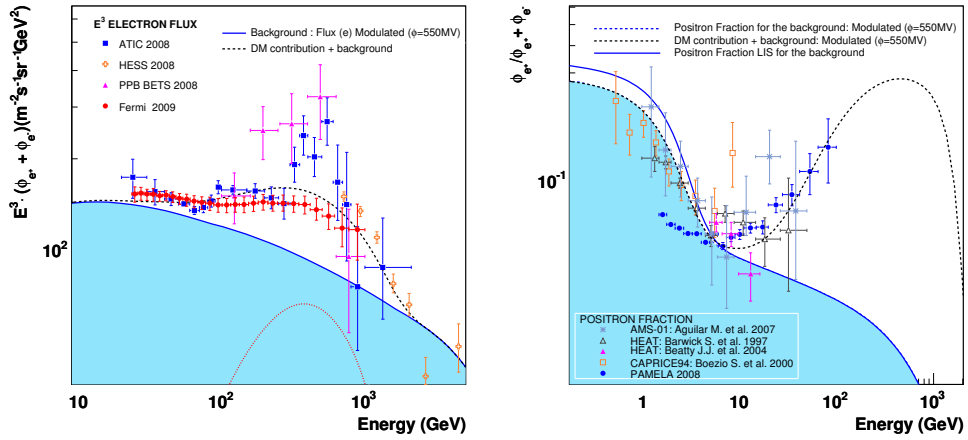

(a) (b)

Figure 5: DM point-like source contribution to the electron spectrum. In each figure the blue solid line stands for the background whereas the black dashed line accounts for the DM contribution over the background to the total flux. The red dashed line denotes the DM contribution to the total flux. The blue dashed line that bounds the blue flooded area denotes a modulated positron fraction for the background. DM clump situated at d=0.9Kpc. MED diffusion setup and luminosity $L = 1.0\text{x}10^{9}\text{M}_{\odot}^{2}\text{pc}^{-3}$. We assume a DM candidate of mass 3.6 TeV that annihilates into $\tau^{+}\tau^{-}$ with cross section $\langle\sigma v\rangle = 3\text{x}10^{-25}\text{cm}^{3}/\text{s}$ (a): $E^{3}\cdot(e^{+}+e^{-})$ (b): Positron Fraction

5. Anisotropies

So far, large scale anisotropies of CR have been measured to be less than 1% [32], but it is known that if they were produced by sources with some spatial structure, small anisotropies should be present in the arrival directions and could be correlated to the potential sources, whether they be known or not. In the case of high energy electrons, very light charged particles, diffusion competes with large energy losses resulting in relatively short paths $\mathcal{O}$(Kpc), so it is expected that we can use them to sample only sources within a certain distance and age. The cosmic ray intensity can, in general, be expanded over the celestial sphere in spherical harmonics. At first order, when we have a marked directionality, we have a dipole anisotropy as could be the case of a single source dominating the spectrum. In this case, the intensity can be expressed as

$$I(\theta) = \bar{I} + \delta\bar{I}\cos\theta \tag{22}$$

where $\bar{I} = 1/2(I_{max} + I_{min})$ being this maximum and minimum intensities related to a forward-backward measurement.

The calculation of the anisotropy produced by a single source has been carried out by [33] and is given by:

$$\delta_i = \frac{3D}{c} \frac{\mid \nabla N \mid}{N} \tag{23}$$

Where $D(E)$ is the diffusion coefficient and N is the electron number density.

In order to detect a statistically significant anisotropy, at the 2σ level, $\delta > 2\sqrt{2}(N_{evts})^{-1/2}$ where N_{evts} is the number of events above a given energy threshold, that is a function of the detector acceptance and the exposition time. $N_{evts}(E > E_{th}) = \int_{E_{th}} \phi(r, E) \cdot Acc \cdot T_{exp} dE$.

Estimates of the expected anisotropy in the case of a dominant pulsar have been previously shown in e.g. [13],[14] but they fail to take into account the possible effects that could arise from a realistic collection of pulsars; there could be e.g. systematic cancellations. We have calculated the anisotropy in the case of a collection of pulsars taken from the ATNF catalogue and, for the first time, in the framework of dark matter annihilation of clumps throughout the halo, both in the case of a dominating point-like source or a distribution of clumps. In the presence of an isotropic background plus a number of contributing sources to the total flux, the expected dipole anisotropy is given by :

$$\delta = \frac{\sum \phi_i(E, r, t) \langle \delta_i \hat{r}_i \hat{n}_i \rangle}{\phi_T} \tag{24}$$

where the index i runs over all the discrete sources that contribute to the full dipole. The product $\langle \delta_i \hat{r}_i \hat{n}_i \rangle$ represents the projection of the individual dipole over the direction of maximum intensity that is energy dependent and $\phi_T(E, r, t)$ denotes the total flux observed at Earth. The projection can be easily calculated taking into account the angular separation θ of two sources on the celestial sphere given by:

$$\theta = \arctan\left(\frac{\sqrt{A1 + A2^2}}{\sin\delta_1 \sin\delta_2 + \cos\delta_1 \cos\delta_1 \cos(\alpha_2 - \alpha_1)} \right) \tag{25}$$

Where $A1 = \cos^2\delta_2 \sin^2(\alpha_2 - \alpha_1)$, $A2 = \cos\delta_1 \sin\delta_2 - \sin\delta_1 \cos\delta_2 \cos(\alpha_2 - \alpha_1)$ and the right ascension and declination are denoted by α_i and δ_i.

In this work, we evaluate the anisotropy (Fig. 6) produced by the collection of pulsars considered in Fig. 2 (a) for a MED diffusion setup.
The dipole anisotropy will change direction depending on the energy, but the main contributor to the full dipole is shown to be Monogem above a few tens of GeV up to the TeV and in second place Geminga. A big contribution to the anisotropy (and the positron flux) can be expected also at higher energies by younger objects like Vela or CTA1, although it is still unclear if such an object can produce a sizeable amount of electrons due to the PWN confinement. The full dipole (Fig. 7) will be given by the projection of the individual anisotropies in the direction of the maximum intensity at each energy, resulting in a clear signal in the direction of Monogem at energies above 20 GeV. The contribution due to Geminga has an addition effect to the full anisotropy due to the relative position between it and Monogem, so, changes in their individual contributions to the flux, codified for instance in the pair conversion efficiency, should not change the anisotropic pattern. Contributions from other pulsars don't result in a systematic addition of their signal to the full anisotropy into a particular direction due to their spatial distribution, so they constitute a kind of isotropic background. In this scenario, measurements of a possible privileged incoming direction should point out an excess in the Monogem/Geminga direction, roughly opposite to the direction of the Milky Way (MW) center. It is possible however that we could be observing the contribution of some yet undiscovered pulsars that could show up in a potential study of anisotropies. In this respect, searches for Gamma-Ray sources as the one conducted by Fermi will help to support or disfavour the test.

In the case of a number of clumps contributing to the full dipole, as in the case of Diemand et al.'s simulation, due to the symmetry of the clump distribution we would expect a dipole anisotropy in the direction of the MW center. The expected dipole anisotropy will be given by

$$\delta = \frac{1}{\phi_T} \int \phi(E, \mathbf{r}) \langle \delta_{clump}(\mathbf{r}) \mathbf{n} \rangle d^3\mathbf{r} \tag{26}$$

where $\langle \delta_{clump}(r) n \rangle = \frac{6D(E)}{cD_{diff}^2}(r_\odot - r\cos\varphi)$ is the projection of the clump contribution to the full dipole in the direction of the MW center and r,φ are the cylindrical coordinates of the clump distribution.

If we introduce the clump distribution we have used in the previous section, the expected dipole anisotropy will be :

$$\delta(E) = \frac{1}{\phi_T}\frac{\beta c}{4\pi}\frac{\langle\sigma v\rangle}{m_{DM}^2}\int_E^\infty dE_s f(E_s)\int r_s dr_s d\varphi_s dz_s \frac{6D(E)}{cD_{diff}^2}(r_\odot - r_s\cos\varphi_s)$$
$$G(\mathbf{r}_\odot, E \leftarrow \mathbf{r}_s, E_s)\int_{M_{min}}^{M_{max}} d\log(M/M_\odot)\frac{dn(r_s,M)}{d\log(M/M_\odot)}f_{NFW}^2(c,M) \quad (27)$$

We can now proceed to estimate the anisotropy that would result from the electron population that fits a given dataset. Throughout this work we have dealt with the PAMELA + Fermi data, as the latter is the most statistically significant, but there is a caveat involved here, namely, the Fermi's energy resolution issue already discussed. This is important because the anisotropic

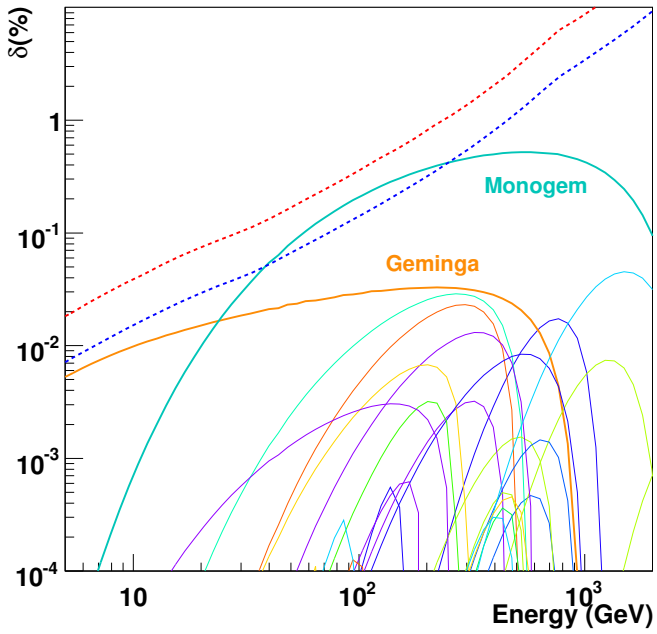

Figure 6: Individual dipole anisotropy in the electron + positron spectrum for every pulsar considered in Fig. 2 (a) and Table 3 for a MED diffusion setup. We also show the Fermi sensitivity to such an anisotropy at the 2 (blue dashed) and 5 (red dashed) σ CL in 5 years.

pattern would be larger in case we had fitted the model to the ATIC data due to a larger flux. Moreover, the dipole that we expect from the clump distribution will be tiny in contrast to a point like source or a dominating source. Taking these facts into account, we estimate the dipole anisotropy for two datasets, namely, PAMELA + Fermi (Fig. 8) and PAMELA + ATIC (Fig. 10). For the former, we have considered the parametrization in Fig. 4, with soft annihilation through $\tau^{\pm}$ and for the latter we have assumed direct annihilation into $e^{\pm}$ in order to reproduce the ATIC bump. From these figures, we can see that in view of the Fermi results, we don't expect a measurable anisotropy for a 5 years survey as the Fermi spectrum is too flat. On the contrary, fits to the much bumpier ATIC data could provide a signature at the 2σ C.L. toward the MW center providing a hint to the origin of the positron excess.

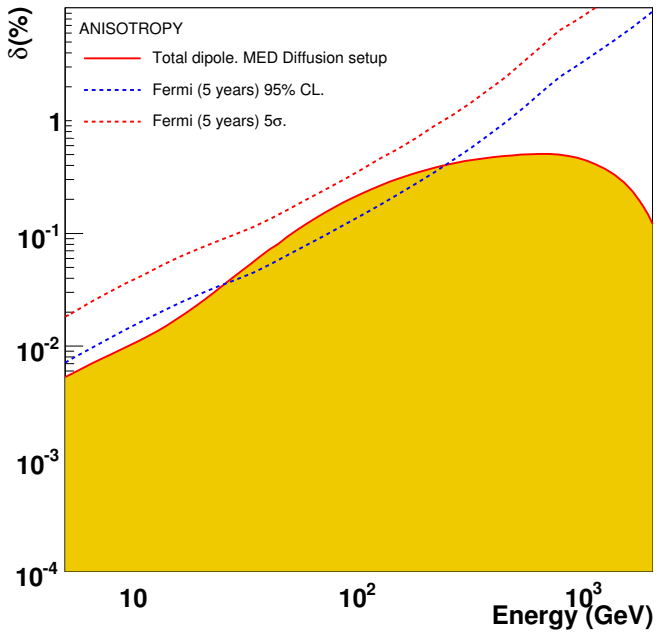

Figure 7: Full dipole anisotropy in the electron + positron spectrum from collection of pulsars as considered in Fig. 2 for a MED diffusion setup. We also show the Fermi sensitivity to such an anisotropy at the 2 and 5 σ CL in 5 years.

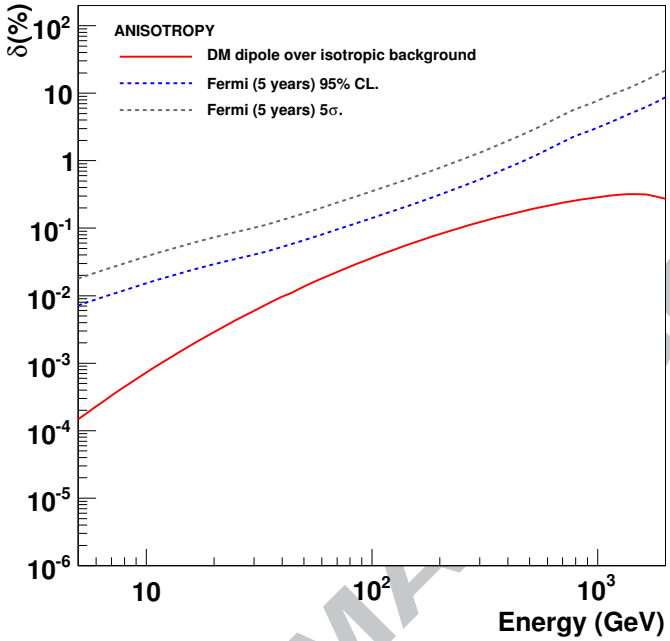

Figure 8: Dipole anisotropy in the electron + positron spectrum from a distributed DM source considered in Fig. 4. We also show the Fermi sensitivity to such an anisotropy at the 2 and 5 σ CL in 5 years.

We can also consider a DM point source as responsible of the bulk of PAMELA and Fermi electrons as could be the case of a large DM clump [31] or minispikes around an intermediate mass black hole [34]. In this case the expected anisotropy is reduced to $\delta = \frac{\phi(E,r)\delta_{pointsource}}{\phi_T}$ where $\delta_{pointsource} = \frac{6D(E)d}{cD^2_{diff}}$ being d the distance to the source (Fig. 9).
Although the probability of finding such a bright clump in our neighbourhood is rather small, there are some scenarios, with the Sommerfeld effect at play, where this probability can be boosted up to 15%. In this case, the anisotropy would exceed the 2σ level pointing toward the existence of a dominant source. This measurement should also be complemented with searches for Gamma-Ray emission to achieve a consistent prediction.

6. Conclusions

A number of possibilities have been proposed as potential candidates to account for the positron excess. From the standard astrophysical point of view, pulsars seem to be the most promising candidates. Just considering the already known Gamma-Ray pulsars is enough to explain the spectrum for reasonable model assumptions, but the features in the ATIC data require quite a large conversion factor into pairs for the considered model. On the other hand, the Fermi data shows a much flatter spectrum that can be reproduced with a reasonable set of pulsar parameters. If we consider dark matter annihilation, the contribution from the clumpy halo can reproduce the observed patterns once we have solved the required normalization issue by means of particle physics boosts on the thermal averaged cross section. In these models, the measured spectrum can be reproduced and no clear

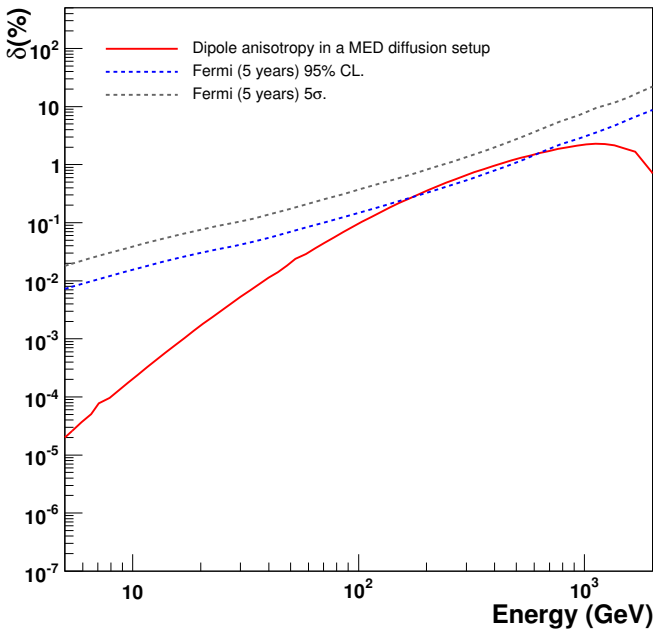

Figure 9: Dipole anisotropy in the electron + positron spectrum from the DM point-like source as considered in Fig. 4. We also show the Fermi sensitivity to such an anisotropy at the 2 and 5 σ CL in 5 years.

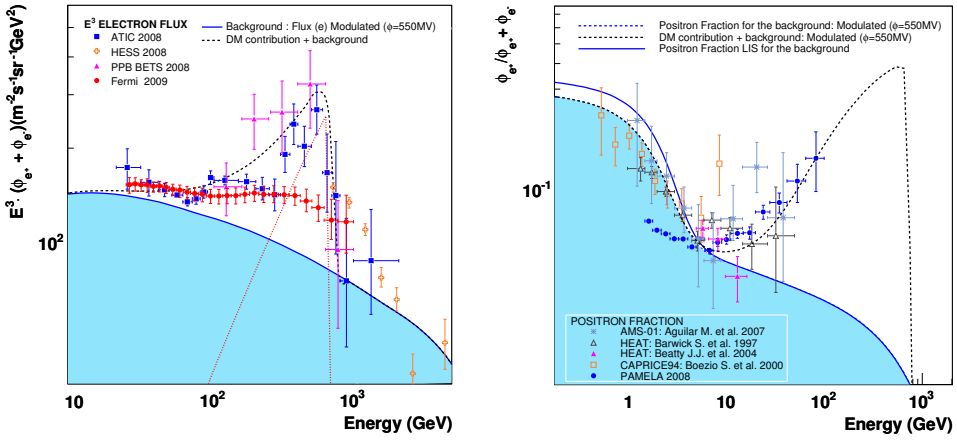

(a) (b)

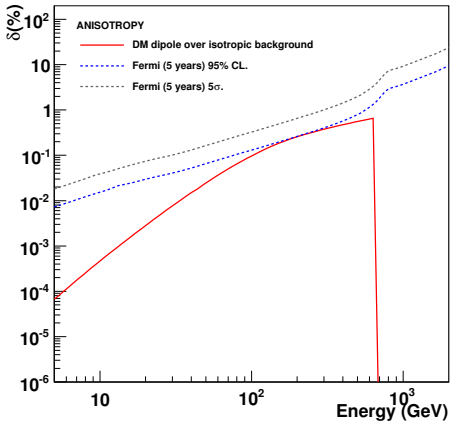

(c)

Figure 10: DM clumpy halo contribution to the electron spectrum. In figures (a) and (b) the blue solid line stands for the background whereas the black dashed line accounts for the DM contribution over the background to the total flux. The red dashed line denotes the DM contribution to the total flux. The blue dashed line that bounds the blue flooded area denotes a modulated positron fraction for the background. Annihilation into e^+e^- with a cross section $\langle\sigma v\rangle = 6.0\text{x}10^{-25}\text{cm}^3/\text{s}$. The considered DM mass $M_{DM} = 680$ GeV and concentration parameter c=1.6. MIN diffusion setup. (a): $E^3 \cdot (e^+ + e^-)$ (b): Positron Fraction (c): Dipole anisotropy in the electron + positron spectrum normalized to the ATIC data for the configuration in (a),(b)

signatures can be found to distinguish between a dark matter scenario and pulsars, as the spectral shape seems to lack information of the origin of the electrons.

In order to distinguish between the proposed candidates, the study of anisotropies is proposed. In this work we have analyzed the expected anisotropy from a configuration of pulsars selected from the ATNF catalogue. We have also derived the anisotropy in a general dark matter scenario, both in the case of a very bright point source and in the case of a clumpy distribution as illustrated by N-body simulations. For the DM point-like source and the pulsar scenarios, the Fermi observatory should be able to detect a dipole anisotropy at 2σ CL in five years at least. On the other hand, we would expect an excess toward the MW center in the case of a clumpy halo as the main contributor to the primary positron flux, but fits to the Fermi spectrum doesn't provide enough events in a 5 years survey. In contrast, the case of the ATIC spectrum would open the possibility of direct annihilation into e^+e^- implying a much harder spectrum. Even annihilations through $\tau^{\pm}, \mu^{\pm}$ channels would imprint a signature in the electron anisotropy detectable by Fermi that are not expected to be observed in view of the the Fermi data.

Anisotropies have been shown to be a valuable tool to disentangle the positron excess problem, nonetheless there are still many of theoretical uncertainties (e.g. the dark matter halo distribution or the mechanism of pair production in pulsars). It must be borne in mind that we have not taken into account the proper motion of the pulsars or even that of the dark matter clumps, which could result in an enhancement or suppression of the anisotropy. Moreover, the case of a dipole anisotropy toward a pulsar cannot exclude a dark matter scenario, as it is possible to have a large dark matter cloud in the same direction masking the signal. In any case, the precise study of electron anisotropies should be conducted together with pulsar surveys to help to discriminate between astrophysical and more exotic sources.

7. Acknowledgements

I would like to acknowledge the support from Javier Berdugo, Carlos Mañá, Jorge Casaus and Carlos Delgado for their useful suggestions and endless patience and Aurelio Carnero for the proofreading. I would also like to thank D.Grasso, D.Gaggero and G.DiBernado for their useful remarks and the anonymous referee for his helpful comments. This work is partially supported by the Centro de Investigaciones Energéticas, Medioambientales

y Tecnológicas (CIEMAT) and the MICINN FPI Grant number BES-2007-151967.

References

[1] O. Adriani, et al., An anomalous positron abundance in cosmic rays with energies 1.5-100 GeV, Nature 458 (7238) (2009) 607–609.

[2] J. Chang, et al., An excess of cosmic ray electrons at energies of 300-800 GeV, Nature 456 (2008) 362–365.

[3] S. Torii, et al., High-energy electron observations by PPB-BETS flight in Antarctica, arXiv:0809.0760.

[4] FERMI/LAT collaboration, Measurement of the Cosmic Ray e+ plus e-spectrum from 20 GeV to 1 TeV with the Fermi Large Area Telescope, Phys. Rev. Lett. 102 (18).

[5] S. W. Barwick, et al., Measurements of the Cosmic-Ray Positron Fraction from 1 to 50 GeV, Astrophys. J. 482 (1997) 191–194.

[6] M. Aguilar, et al., Cosmic-ray positron fraction measurement from 1 to 30 GeV with AMS-01, Physics Letters B 646 (4) (2007) 145–154.

[7] T. Delahaye, R. Lineros, F. Donato, N. Fornengo, J. Lavalle, P. Salati, R. Taillet, Galactic secondary positron flux at the Earth, Astronomy and Astrophysics 501 (3) (2009) 821–833.

[8] M. Cirelli, M. Kadastik, M. Raidal, A. Strumia, Model-independent implications of the e+, e-, anti-proton cosmic ray spectra on properties of Dark Matter, Nucl. Phys. B813 (2009) 1–21.

[9] V. Ginzburg, S. Syrovatskii, The origin of cosmic rays, Pergaemon, Oxford, 1964.

[10] I. V. M. Andrew W. Strong, V. S. Ptuskin, Cosmic-ray propagation and interactions in the Galaxy, Annual Review of Nuclear and Particle Systems vol. 57 (1) (2007) 85–327.

[11] T. Delahaye, R. Lineros, F. Donato, N. Fornengo, P. Salati, Positrons from dark matter annihilation in the galactic halo: Theoretical uncertainties, Physical Review D 77 (6).

[12] A. K. Harding, R. Ramaty, The Pulsar Contribution to Galactic Cosmic Ray Positrons, in: International Cosmic Ray Conference, Vol. 2 of International Cosmic Ray Conference, 1987, pp. 92–+.

[13] I. Büsching, O. C. de Jager, M. S. Potgieter, C. Venter, A Cosmic-Ray Positron Anisotropy due to Two Middle-Aged, Nearby Pulsars?, ApJ 678 (1) (2008) L39–L42.

[14] D. Hooper, P. Blasi, P. Serpico, Pulsars as the Sources of High Energy Cosmic Ray Positrons, Journal of Cosmology and Astroparticle Physics 1 (2009) 25–+.

[15] H. Yüksel, M. D. Kistler, T. Stanev, TeV Gamma Rays from Geminga and the Origin of the GeV Positron Excess, Phys. Rev. Lett. 103 (5) (2009) 051101.

[16] X. Chi, K. S. Cheng, E. C. M. Young, Pulsar-Wind Origin of Cosmic-Ray Positrons, ApJ 459 (2) (1996) L83–L86.

[17] Q. Gao, Z. Jiang, L. Zhang, Possible Contribution of Mature Gamma;-Ray Pulsars to Cosmic-ray Positrons, Chinese Journal of Astronomy and Astrophysics 8 (1) (2008) 87–95.

[18] S. Profumo, Dissecting Pamela (and ATIC) with Occam's Razor: Existing,well known Pulsars naturally account for the "anomalous" Cosmic-Ray Electron and Positron Data, arXiv:0812.4457.

[19] D. Grasso, et al., On Possible Intepretations of the high Energy Electron-Positron Spectrum measured by the Fermi Large Area Telescope, Astroparticle Physics 32 (2) (2009) 140–151.

[20] L.Zhang, K.S.Cheng, Cosmic-ray positrons from mature gamma-ray pulsars, A&A 368 (3) (2001) 1063–1070.

[21] R. N. Manchester, G. B. Hobbs, A. Teoh, M. Hobbs, The ATNF pulsar catalogue, Astron. J. 129 (2005) 1993–2006.

[22] L. Zhang, K. Cheng, High-Energy Radiation from Rapidly Spinning Pulsars with Thick Outer Gaps, ApJ 487 (1) (1997) 370–379.

[23] D. Thompson, et al., EGRET high-energy gamma-ray pulsar studies. 1: Young spin powered pulsar., ApJ 436 (1) (1994) 229–238.

[24] N. Kawanaka, K. Ioka, , M. M. Nojiri, Is cosmic-ray electron excess from pulsars is spiky or smooth? continuous and multiple electron/positron injections, The Astrophysical Journal 710 (2) (2010) 958–963.

[25] A. M. Atoyan, F. A. Aharonian, H. J. Völk, Electrons and positrons in the galactic cosmic rays, Phys. Rev. D 52 (6) (1995) 3265–3275.

[26] D. Malyshev, I. Cholis, J. Gelfand, Pulsars versus dark matter interpretation of ATIC/PAMELA, Phys. Rev. D 80 (6) (2009) 063005.

[27] J. Diemand, B. Moore, J. Stadel, Earth-mass dark-matter haloes as the first structures in the early universe, Nature 433 (2005) 389–391.

[28] D. Cumberbatch, J. Silk, Local dark matter clumps and the positron excess, MNRAS 374 (2) (2006) 455–465.

[29] E. Baltz, A. Edsjo, Positron propagation and fluxes from neutralino annihilation in the halo, Phys. Rev. D 59 (2) (1998) 023511.

[30] P. Meade, M. Papucci, A. Strumia, T. Volansky, Dark Matter Interpretations of the Electron/Positron Excesses after FERMI, arXiv:0905.0480.

[31] P. Brun, T. Delahaye, J. Diemand, S. Profumo, P. Salati, Cosmic ray lepton puzzle in the light of cosmological n-body simulations, Phys. Rev. D 80 (3) (2009) 035023.

[32] Amenomori, et al., Anisotropy and corotation of galactic cosmic rays, Science 314 (5798) (2006) 439 – 443.

[33] C. Mao, C. Shen, Anisotropy and diffusion of cosmic ray electrons, Chinese Journal of Physics 10 (1) (1971) 16–28.

[34] T. Bringmann, J. Lavalle, P. Salati, Intermediate mass black holes and nearby dark matter point sources: A critical reassessment, Phys. Rev. Lett. 103 (16) (2009) 161301.

Pulsar Name	d[Kpc]	T [10^5 years]	$\dot{E}$ [10^{34} erg/s]
J0633+1746	0.16	3.42	3.2
B0656+14	0.29	1.11	3.8
B0833-45	0.29	0.11	690.0
B0355+54	1.10	5.64	4.5.0
J2043+2740	1.13	12	5.6.0
J1740+1000	1.36	1.14	23.0
J0538+2817	1.39	6.18	4.9
B1055-52	1.53	5.35	3.0
J1549-4848	1.54	3.24	2.3
B1706-44	1.82	0.18	340
B1449-64	1.84	10.40	1.9
B0740-28	1.89	1.57	14.0
B0114+58	2.14	2.75	22.0
J0821-4300	2.20	14.90	3.3
J1046+0304	2.25	4.16	1.4
B1221-63	2.29	6.92	1.9
B2334+61	2.47	0.41	6.2
J1747-2958	2.49	0.26	250.0
B1951+32	2.50	1.07	370.0
B1719-37	2.51	3.45	3.3
J1830-0131	2.68	11.50	2.3
B0136+57	2.70	4.03	2.1
J1028-5819	2.76	0.90	83.0
B1046-58	2.98	0.20	200.0

Table 3: Gamma-Ray Pulsars from the ATNF Catalogue. A subset from the collection of pulsars in the database is listed with d $<$ 3Kpc and 10^4 years $<$ T $<$ 10^7 years.